Conduit flow experiments help constraining the regime of explosive eruptions

P. Dellino[1], F. Dioguardi[1], B. Zimanowski[2], R. Büttner[2], D. Mele[1], L. La Volpe[1], R. Sulpizio[1], D. M. Doronzo[1], I. Sonder[2], R. Bonasia[3], S. Calvari[4], E. Marotta[3]

[1]Centro Interdipartimentale di Ricerca sul Rischio Sismico e Vulcanico (CIRISIVU) – c/o Dipartimento Geomineralogico, Università di Bari, Via E. Orabona 4, 70125 Bari, Italy

[2]Physikalisch Vulkanologisches Labor,Universität Würzburg, Pleicherwall 1, 97070, Würzburg, Germany

[3] Osservatorio Vesuviano, Istituto Nazionale di Geofisica e Vulcanologia, 80124, Napoli, Italy

[4] Istituto Nazionale di Geofisica e Vulcanologia, Sezione di Catania, 95123, Catania, Italy

P. Dellino corresponding author dellino@geomin.uniba.it

Abstract

It is currently impractical to measure what happens in a volcano during an explosive eruption, and up to now much of our knowledge depends on theoretical models. Here we show, by means of large-scale experiments, that the regime of explosive events can be constrained based on the characteristics of magma at the point of fragmentation and conduit geometry. Our model, whose results are consistent with the literature, is a simple tool for defining the conditions at conduit exit that control the most hazardous volcanic regimes. Besides the well-known convective plume regime, which generates pyroclastic fallout, and the vertically collapsing column regime, which leads to pyroclastic flows, we introduce an additional regime of radially expanding columns, which form when the eruptive gas-particle mixture exits from the vent at overpressure with respect to atmosphere. As a consequence of the radial expansion, a dilute collapse occurs, which favours the formation of density currents resembling natural base surges. We conclude that a quantitative knowledge of magma fragmentation, i.e. particle size, fragmentation energy and fragmentation speed, is critical for determining the eruption regime.

Introduction

Velocity, density and cross sectional area of the gas-particle flows issuing from volcanic conduits are the main quantities controlling the eruption rate and the regime of explosive events [*Wilson et al., 1980; Woods, 1988; Bursik and Woods, 1991*]. They are generally subdivided into two main categories: convective plumes and collapsing columns. Detailed knowledge of these quantities is a fundamental prerequisite for hazard assessment, because different regimes lead to different eruption styles: i.e. pyroclastic fallout vs. pyroclastic density currents, which possess very different damage potentials over a territory or population. Since it is difficult to measure conduit conditions during eruptions directly, much of our information on the conduit flow conditions leading to different regimes comes from theorethical models [*Woods, 1995a; Koyaguchi and Mitani, 2005*], numerical simulations [*Valentine and Wohletz, 1989; Dobran et al., 1993; Papale, 2001*] and empirical relations developed in engineering [*Ishii and Zuber, 1979; Garic et al, 1995*]. Model validation has been a difficult task in volcanology [*Burgisser et al., 2005*], because the few relevant laboratory experiments were of small scale and did not make use of natural volcanic materials. To help address this shortfall, we present here new data on large-scale experiments of conduit flows, which were carried out with natural materials from pyroclastic deposits. The aim of the paper is to: 1) investigate the influence of pyroclast characteristics, gas pressure and conduit geometry on the exit conditions leading to different regimes; 2) apply our experimental model to natural conditions and compare results with literature data; and 3) construct new diagrams in which magma characteristics at the point of fragmentation and conduit geometry are used to define stability fields for different regimes.

Experimental apparatus and methods

Gas-particle coupling is strongly influenced by the peculiar morphology of volcanic particles [*Dellino et al., 2005*], so we designed the experiment at a scale large enough to allow the use of real eruption products. The set-up (Fig. 1A), described in detail by *Dellino et al.*, [*2007*], consists of a conduit that is loaded with samples of up to 220 kg of pyroclastic deposits from Vesuvius, Mount Vulture and Etna (southern Italy). The grain-size distribution ranges from a median size of 0.5 ϕ (0.71mm) with a sorting value of 2.5 ϕ to a median size of -0.6 ϕ (1.5 mm) with a sorting value of 1ϕ. This means that the particle load of the experiment includes a broad range, from fine ash to medium lapilli. We used conduit diameters, *D*, of 0.6 and 0.3 m, while conduit length, *L*, ranged from 0.55 m to 3.2 m. Nozzles in the base plate of the conduit are connected to a high-pressure gas volume by means of steel reinforced rubber tubes. Opening of fast solenoid valves results in the mechanical coupling of released gas and pyroclasts (Fig. 1B).

Experiments were performed both at ambient temperature and up to 300°C, and thermal videocameras were used to monitor the eruptive flow and check the influence of temperature for the evolution of the external flow.

We measured experiments at a high sampling rate with a network of pressure sensors and digital video cameras. The experimental set-up and the network of sensors were arranged so as to allow the measurement of the main quantities that influence initiation, evolution and exit conditions of the gas-particle conduit flow.

The conduit exit velocity of the gas-particle mixture, W_{exit}, was measured by means of frame-by-frame analysis of the digital sequences captured by video cameras. The high definition format (720x1280 pixels) allowed discretization of the scene at conduit exit at a scale lower than 0.01m/pixel, so the precision of distance measurements was about +/- 0.005m. The recording rate of 50 frames per seconds resulted in a typical translation distance of the gas-particle mixture between two successive frames at the conduit exit (depending on exit velocity) of about 0.5m. The relative error on distance measurement between two successive frames is therefore about +/- 1%. Error of the time interval between two successive frames is linked to precision of the internal digital clock of video cameras, and is insignificant compared to distance error. Overall, the relative error of velocity measurements is about +/- 1%.

The total mechanical energy (E_{totexp}) that can be transferred from the driving pressure of the reservoir to the particle load is known, because initial gas overpressure, ΔP_{init}, and reservoir gas volume V_{ginit}, are known.

The driving pressure history, which is recorded by a transducer placed between the gas reservoir and the nozzles (Fig. 1B), was measured at a 10 kHz sampling rate by a Kistler™ absolute pressure sensor, which has a certified relative error of +/- 0.3%. The driving pressure history is used to monitor the mechanical energy transferred over time from the gas to the particle load. The total area under the curve of the pressure gradient over time is directly proportional to the total mechanical energy, so the area enclosed over a certain time interval can be used to calculate the amount of mechanical energy transferred over that time interval.

Pressure inside the conduit was recorded by means of transducers placed perpendicular to flow direction, in a configuration that allowed the measurement of gas pressure during the passage of the gas-particle mixture along the conduit (Fig. 1C). It was recorded at a 1kHz sampling rate by Sika™ relative pressure sensors, which have a certified relative error of +/- 0.25%. Pressure data, both from the driving pressure and the conduit were all processed at 1kHz for homogeneity of data analysis.

During the experiments, we wanted to measure the amount of mechanical energy needed to accelerate the gas-particle mixture in the conduit, which in many natural events is coupled with magma fragmentation processes. This is because most powerful explosive eruptions involve stress-induced brittle magma fragmentation occurring at some depth in the conduit [*Dingwell, 1996; Papale, 1999; Büttner et al., 2006*]. In this fragmentation process, once the melt is stressed beyond a certain critical value by a pressure differential, it undergoes brittle fragmentation, which results in the release of mechanical energy that accelerates the gas-particle mixture [*Büttner et al., 2006*]. Since our main intent was to investigate this type of eruptions, our set-up was designed so that experimental data on the mechanical energy released upon magma fragmentation could be used as an initial condition for the gas-particle flow acceleration in the conduit flow. This is an impulsive process, so it was necessary to verify that the time for coupling of stress to magma during fragmentation experiments was in the same range as stress was coupled from the driving pressure before the particle load started to move in our experiments. This was achieved by ensuring that the time scale of driving pressure coupling to the particle load before initiation of particle acceleration in the conduit was in the same range as the time scale of stress build-up before magma fragmentation in fragmentation experiments [*Büttner et al., 2006*]. To measure the amount of mechanical energy transferred from the driving pressure to initiate acceleration of the gas-particle mixture in the conduit, we used a pressure sensor placed near the conduit base, at a level that is completely filled with particles (Fig. 1C). By matching the driving pressure history with the timing of the pressure peak registered at this sensor at the initiation of particle motion (system expansion), the mechanical energy transferred from the driving pressure into the particle mass and then impulsively released upon system expansion was calculated (Fig. 2). It is analogous to the mechanical energy released after magma fragmentation in fragmentation experiments [*Büttner et al., 2006*], so we call it fragmentation energy, $E_{fragexp}$.

Following the initiation of particle acceleration, the continuous release of gas from the pressurized tubes sustains the gas-particle flow along the conduit, similarly to what happens with the expansion of gas liberated from broken vesicles in natural magmas. Since the driving pressure signal is synchronized with the video recording, it is possible to calculate the mechanical energy transferred before the gas-particle mixture issues from the conduit, by calculating the area under the driving pressure gradient between the start of the experiment and the time of conduit exit (Fig. 2). We call this the exit energy, E_{exit}.

In a few dedicated experiments, performed with a conduit length > 2 m, a dense network of pressure sensors was mounted at regular height intervals along the conduit (Fig. 1C). They allowed monitoring of in-conduit flow evolution.

When the load of particles is very high (Fig. 2), the particle volumetric concentration, C, of the gas-particle mixture is high and there is little percolation of gas to the upper part of the conduit during upward motion of the gas-particle mixture (Fig. 3A). In this case, the pressure peak recorded from a pressure sensor registers the passage of the gas-particle flow front at the sensor location. Thus, the time-lag between the pressure peak of two successive sensors, divided by the distance between the sensors, is a measure of the speed of the flow front, which is actually the velocity of the gas-particle mixture. It is evident from Fig. 2 that, after a short acceleration, velocity stays quite constant along the conduit and it is very similar to the one recorded by videocameras at conduit exit. For conduit lengths >1m, the gas-particle flow rapidly reaches a constant velocity that is maintained until conduit exit. By using a conduit much shorter than 1 m, unsteady conditions are produced. In this case, exit velocity is lower and exit overpressure much higher.

When, instead, the particle load is lower, particle volumetric concentration in the gas-particle mixture is lower and gas effectively percolates through the gas-particle mixture higher in the conduit (Fig. 3B). In this case, the time-lag between the pressure peak at different sensors is a measure of the speed at which pressure waves travel along the conduit, which, if calculated when the mixture reaches conduit exit, is actually a measure of the speed of sound of the gas-particle mixture (Fig. 4). In the case of the experiment of Fig. 4a this value is about 27 m/s, which is quite low, but is consistent with the low speed of sound that is expected with gas-particle mixtures with particle volumetric concentration, *C*, of a few percent. In particular, if we assume that the mixture is well homogenized and the concentration is $C=V_p/V$, where V_p is particle volume and V is conduit volume where $V=V_g+V_p$ (total conduit volume including particles), in the case of the experiment of Fig. 4A, *C* is about 0.12. This value of concentration, when matched with the calculated value of speed of sound, is consistent with the dependence of the speed-of-sound on particle volumetric concentration [*Wohletz, 1998*]. We can thus conclude that our way of calculating particle volumetric concentration is a good approximation of the bulk particle volumetric concentration. Other, hot runs, with still lower concentration (0.04), show a speed of sound of the mixture of about 110 m/s (Fig. 4B). This is, again, consistent with what postulated for multiphase flows, which is that, by lowering concentration and increasing temperature, the speed of sound of a gas-particle mixture increases significantly.

By matching the speed of sound of the gas-particle mixture with exit velocities, it emerges that during the experiments, at the conduit exit the Mach number was in between 0.3 (for dilute runs) to 0.5 (for concentrated runs). Therefore the conduit flow was always sub-sonic. Nevertheless, at conduit exit a gas pressure by far exceeding atmospheric pressure was registered in some concentrated runs. This means that the overpressure at conduit exit is to be attributed probably to the fact that the mixture was not highly permeable and gas didn’t percolate much throughout the conduit during travel of the flow. We therefore demonstrate that overpressure can be reached not only when chocked flow conditions are reached in the conduit but also when high particle concentration in the mixture is maintained up to conduit exit.

Since the conduit exit velocity is taken by videocameras, it is actually a measure of the particles’ velocity in the gas-particle mixture. The velocity difference between gas and particles in a multiphase gas-particle mixture is called slip velocity and is represented by the terminal velocity of particles in the mixture. We calculated the terminal velocity, *w*, of our particles by the experimental model proposed by Dellino et al. [2005],

$$w = \frac{1.2065\mu_{mix}(d^3 g(\rho_{part} - \rho_{mix})\rho_{mix}\Psi^{1.6} / \mu_{mix}{}^2)^{0.5206}}{d\rho_{mix}} \quad (1)$$

in which Ψ is particle shape factor, which in our case is about 0.4; μ_{mix} is mixture viscosity, ρ_{part} is particle density, ρ_{mix} is mixture density, *g* is gravity acceleration and *d* is particle diameter. For high concentration runs (C=0.2) terminal velocity of 0.7 mm particles (typical median size of the diameter of the experimental particle population) is of 0.127 m/s and for 0.064 mm particles (typical fine ash component in our experimental particle population) is about 0.03 m/s. In the case of dilute runs (C=0.04) the terminal velocity of a 0.7 mm particle is of 0.3 m/s and it is of 0.08 m/s for particles of 0.064 mm. Since the typical velocities measured in our experiments are in the order of 10 m/s, this means that the slip velocity is always much smaller than gas velocity. Therefore, if in our experiments we assume that the gas-particle mixture velocity is well approximated by particle velocities, we make an error of less than 1.3 % for concentrated flows and of 3% for dilute flows. In this research we thus assume that particle velocity represents an acceptable approximation of the gas-particle mixture velocity. Naturally, in the real eruptive case, with very long conduits, and especially inside highly dilute atmospheric plumes, fine particles are much more coupled to gas then coarse ones. In that case the difference in slip velocity between coarse and fine particles can be significant and effective in segregating particles by their size during atmospheric transportation and deposition.

The gas-particle mixture does not show visible inhomogeneities at conduit exit, and the pressure curves are smooth (Fig. 2). This evidence is in contrast with conduit flows reported from pneumatic engineering, which are generally described as a discontinuous progression of particle slugs [*Mader et al., 1996; Crowe, 2006*]. This effect may not be evident in our case because conduit diameter is quite large and attenuates slug formation [*Crowe, 2006*].

In order to check the combined influence of particle characteristics, energy and conduit geometry on the eruptive regime, experiments were performed over a wide range of conditions (see table 1) of initial gas overpressure, ΔP_{init}, initial gas volume, V_{ginit}, conduit diameter, D, conduit length, L, mass m, and grain size of particles, d_p, where d_p represents particle median diameter normalized to 1 mm.

Illustration of experimental regimes

By varying conditions, different regimes resembling natural explosive eruptions were replicated by our experiments. In particular, by changing the ratio (which we call specific mechanical energy, *SME* [*Dellino et al., 2007*]) between the total mechanical energy, E_{totexp}, and mass of particles, m, it was possible to generate two main experimental regimes: convective plumes and vertically collapsing columns. Dilute convective plumes leading to particle fallout were produced when *SME* was higher than 2.6 kJ/kg (Fig. 5). When it was lower than 1.5 kJ/kg, dense vertically collapsing columns were obtained, which produced, upon contact onto the ground, density currents resembling natural pyroclastic flows (Fig. 6). Intermediate values led to transitional columns where part of the material collapsed and part was convected. In addition, by increasing gas driving pressure and shortening conduit length, a higher overpressure with respect to atmosphere and a lower velocity resulted at conduit exit. In extreme cases, (conduit length of 0.55m) radially expanding columns led to an expanded collapse that generated density currents resembling natural base surges (Fig. 7).

A comparison between cold and hot experiments revealed that heat did not play a decisive role in determining the type of eruptive regime. Convective plumes were produced both with cold and hot experiments (Fig. 8), provided that particle volumetric concentration was lower and exit velocity higher. Higher temperatures in the hot experiments increased convection after the plume was well formed, and it facilitated a further expansion of the upper part of the plume by increased buoyancy, as it is evident from images taken from thermal cameras (Fig. 8). This is probably due to the fact that the time needed to establish thermal convection is much longer than the time needed for the establishment of forced convection at conduit exit, which is more important for allowing initial air entrainment and initiation of the plume. The formation of collapsing columns is also not much affected by temperature. They form, provided that particle volumetric concentration is higher and exit velocity lower, in both cold and hot experiments. Temperature is not decisive for the formation of the density currents upon column collapse. The only difference is that, in the hot pyroclastic flows, the upper part of the current tends to become buoyant more quickly, as expected in the natural case, but the velocity of the shear current at the flow base, where much of the mechanical energy of the flow is contained [*Dellino et al., 2007*], is not much influenced by temperature.

Sensors and dedicated videocameras were placed also along the runout of density currents, in order to record flow evolution. Deposits left by the currents were sampled over the dispersal area to check their features for comparison with natural deposits. The analysis of the evolution of density currents after collapse and comparison of deposit features with those of natural pyroclastic deposits is beyond the scope of the present paper, and is the subject of further research. A general idea can be obtained from *Dellino et al.,* [*2007*], in which a first description of the various phases and evolution with runout distance of the experimental pyroclastic density currents is reported.

Since the focus of the present paper is on the conduit flow and the dependence of eruptive regime on conduit exit conditions, we next deal with how the experimental data were elaborated to develop a model based on the characteristics of: pyroclastic material (mass, grain size and density); gas initial conditions (gas volume and overpressure); data measured from sensors (mechanical energy of fragmentation, mechanical energy transferred before conduit exit); data from videocameras (exit velocity) and conduit geometry (diameter and length).

Experimental model

In order to obtain quantities that could effectively discriminate between the different eruptive regimes produced by our experiments, and that could also have a value for the natural case, we combined data at conduit exit in order to form parameters that have a physical meaning also for explosive eruptions. The list of symbols is reported in table 2.

Concerning a distinction between convective plumes and vertically collapsing columns, we know that exit velocity is an important factor, since higher velocities favour convective plumes. Also, we know that particle volumetric concentration is important since a lower concentration at conduit exit could allow further expansion of the column with height thus favouring plumes. Finally, conduit radius must be considered, because lower values tend to favour plumes. This is because the ratio of column surface area to volume is important in controlling expansion of the column through entrainment of surrounding air, which favours convective plumes. The higher the ratio, the more effective is entrainment of air in diluting the plume. If we consider a cylindrical column at conduit exit, this ratio is a function of $2/R$, where R is conduit radius. We combined these factors by placing the ones favouring plumes in the numerator, and those favouring collapses in the denominator. The ratio $2W_{exit}/RC$ was so formed, which we calculated for all the experimental runs. As expected, higher values characterized convective plumes and lower values favoured vertically collapsing columns. The reason this parameter is able to discriminate between the two regimes is revealed in its physical meaning. It has dimension of s^{-1} and therefore it can be interpreted as a sort of vorticity factor, which we call Ω. It can be tentatively explained as the tendency of the mixture to be sustained by vortices, which are favoured by lower particle concentration, as is postulated for multiphase flows [*Kulick et al., 1994*]. In our experiments, the limit between convective plumes generating particle fallout and vertically collapsing columns generating pyroclastic flows is about 500 s^{-1}.

In order to form radially expanding columns, gas overpressure with respect to atmosphere is an important factor in allowing lateral expansion. In addition, to favour a significant radial expansion over a vertical one, this overpressure should be significant when compared to the pressure component allowing vertical movement, which is the dynamic pressure, $P_{dyn}=0.5\rho_{mix} W_{exit}^2$, along the vertical axis. A ratio of overpressure and dynamic pressure, P_{over}/P_{dyn}, should thus express the tendency to favour lateral expansion, with higher values allowing for the formation of radially expanding columns. Dynamic pressure was calculated by assuming that mixture density is related to particle volumetric concentration by $\rho_{mix}= \rho_{part}C+\rho_{gas}(1-C)$. This parameter, which we call overpressure factor, Γ, is actually higher for laterally expanding columns, with the threshold separating vertically collapsing columns from radially expanding columns being about 0.3.

A diagram plotting the vorticity and overpressure factors (Fig. 9) for all the experimental runs distinguishes these regimes. An undefined region is found on the right top part of the diagram, where in principle highly overpressured columns with high vorticity, which are not formed in our experiment, should exist. We suspect that the existence of this undefined region is more theoretical than actual, because it is hard to imagine that a highly dilute mixture could maintain a very high gas overpressure at conduit exit.

Since we know that exit velocity is key for the discrimination between different regimes, we analyzed its dependence on quantities that are relevant for the initiation and evolution of the experimental conduit flows, and play also a role in actual eruptions. Comparison between our cold and hot experiments shows that temperature, even though it is important for the later stages of particle dispersion, especially in the case of convective plumes, is not decisive for the inception of the eruptive regime. For this reason, we treated the conduit flow as isothermal [*Papale, 2001, Buresti and Casarosa, 1989*], and analysed experimental data from a simple mechanical point of view. We postulate that exit velocity is influenced by the mechanical energy transferred from the gas to the particles and by conduit geometry. Since kinetic energy is $1/2\ mW_{exit}^2$, we searched for a functional relation of kinetic energy per unit mass, $W_{exit}^2/2$, with the idea of including in the independent variable the mass of particles and all other quantities influencing velocity; these are geometry of the conduit and energy transferred to the particle load from the driving pressure. The best model (Fig. 10A), capturing behaviour in all experiments, including the unsteady cases, is expressed by the following equation

$$W_{exit}^2 / 2 = 16564 + 0.3115\left(\frac{D}{L}\frac{E_{frag\exp}}{P_{atm}V_p d_p (P_{exit}/P_{atm})^{2.5}}\frac{E_{exit}}{m}\right) \quad (2)$$

which has a correlation coefficient, *r*, of about 0.99. The model is a linear function of the general form $y=a+bx$, where *a*, the intercept, has dimensions of m^2/s^2, which are the same as the dependent variable, *y*; *b*, the slope, is a number, and *x*, the independent variable, has the same dimensions as the dependent variable. Since the dependent and independent variables are expressed in the same units, a discussion of the terms contained in the independent variable can help in interpreting the physical meaning of the functional relation. The independent variable actually comprises three factors, each being a ratio, where quantities that are directly proportional to exit velocity appear in the numerator, and quantities that are inversely proportional to exit velocity in the denominator. The first factor, *D/L*, relates to conduit geometry, meaning that with increasing *D* velocity increases, and with increasing *L* velocity decreases. This is what is postulated in fluid dynamics for a conduit flow with a constant pressure gradient sustaining the flow of a viscous fluid. In the second factor of the independent variable, fragmentation energy appears in the numerator, which means that by increasing it, exit velocity increases. This is what we expect, since this quantity is responsible for the initiation of acceleration of the gas-particle flow, as was discussed in an earlier section. The terms P_{atm}, V_p, d_p, and the ratio P_{exit} /P_{atm}, which are inversely proportional to exit velocity, appear in the denominator. Particle volume decreases exit velocity because it renders particle volumetric concentration higher. Particle diameter decreases exit velocity of the gas-particle mixture because coarser particles are less coupled to the gas, so gas tends to escape more easily from the gas-particle mixture, which lags behind. The ratio P_{exit} /P_{atm}, is important because the higher the exit pressure is with respect to atmosphere, the lower the exit velocity will be, since, if there is high overpressure in the gas-particle mixture at conduit exit, it means that not much of the "potential" energy of the gas has been transformed in to kinetic energy. The last factor of the independent variable, E_{exit}/m, is relevant because the higher the energy transferred per unit mass before conduit exit, the higher the exit velocity will be.

This experimental model, due both to its good correlation and to the fact that it is quite easy to interpret, looks satisfying and consistent for showing the potential of our conduit flow model. It is expressed in terms of quantities that can be hypothesized or, at least reasonably inferred for natural eruptions (D, L,V_p, d_p, m, $E_{fragexp}$), but it also includes two quantities, E_{exit} and P_{exit}, which were measured during experiments but are very hard to state for natural eruptions. To address this issue, we looked for additional functional relations allowing the exit energy and exit pressure calculation in terms of other quantities, which could be more easily inferred or hypothesized for natural eruptions.

We searched for a functional relation with exit energy in which to include the total mechanical energy, conduit aspect ratio, particle concentration and size. The best model (Fig. 10B) is given by the following equation

$$E_{exit} = -1750.9 + 0.1275\left(E_{tot\,\mathrm{exp}}\frac{L}{D}C^{\frac{1}{3}}d_p^{\frac{1}{3}}\right) \quad (3)$$

It is also a linear function of the form $y=a+bx$, where a, the intercept, has the same dimensions as the dependent variable, y, while b, the slope, is a number and x, the independent variable, has the same dimensions as the dependent variable. Correlation is good, with *r* about 0.99. An analysis of the terms in the independent variable shows that total energy is directly proportional to exit energy and conduit length, because, other terms being constant, a higher amount of mechanical energy is transferred to move the gas-particle mixture at the conduit exit for a longer conduit. Conduit diameter is inversely proportional to exit energy, since a larger conduit means reduced pressure loss due to conduit friction for the same amount of particles. The higher the concentration, the higher the amount of energy transferred before conduit exit, because the amount of energy loss to particle-particle and particle-conduit friction is higher. The larger the particle size, the higher the energy transferred because gas-particle coupling is influenced by particle size, with coarser particles being less coupled than finer particles, as discussed in an earlier paragraph.

We wanted to obtain a functional relation including conduit geometry to describe exit pressure, in order to have a model able to reconstruct pressure as a function of height. We therefore could use only data from the few experiments for which we had a dense network of pressure sensors placed at regular height intervals. In the functional relation we also used other terms that influence pressure loss, i.e. energy transferred before conduit exit, conduit volume, conduit aspect ratio and particle concentration. The best model (Fig. 10C) is represented by the following equation

$$P_{exit} = 94032 + 0.26466\left(\frac{E_{exit}}{V_g}\left(\frac{D}{L}\right)^{\frac{1}{3}} C^{\frac{1}{3}}\right) \quad (4)$$

This again is a linear function with *a*, the intercept, having the same dimensions as the dependent variable; *b*, slope, is a number, and the independent variable has the same dimensions as the dependent variable. There is some scatter in the data, but the correlation coefficient is high, *r* = 0.98, so the model can be judged as a good approximation of exit pressure. The ability to calculate exit pressure is also useful for recognising the conditions leading to high exit overpressure, which favour shock wave formation in the vicinity of the volcanic crater [*Ogden et al., 2008, Wilson et al., 1978*]. Inspection of the independent variable shows that exit energy, conduit aspect ratio, and particle concentration are directly proportional to exit pressure, while conduit volume is inversely proportional because higher conduit volume lead to higher gas expansion up to the conduit exit and, hence, lower exit pressure.

By combining (2), (3), and (4), and particularly by substituting into equation (2) the exit energy resulting from equation (3) and the exit pressure resulting by combination of (3) and (4), we finally obtained a model of exit velocity that is a function of quantities that can be inferred or reasonably hypothesized in natural eruptions, which are: total energy, fragmentation energy, conduit diameter, conduit length, particle size, particle mass and particle volume. The model is represented by the following equation

$$\begin{aligned}W_{exit} = 1.4142(16.564 + E_{frag}(-545.4D + 0.039712C^{1/3}{d_p}^{1/3}E_{tot}L)(md_pLP_{atm}V_p(94032 + \\ +(0.26466C^{1/3}(D/L)^{1/3}(-1750.9 + (0.1275C^{1/3}{d_p}^{1/3}E_{tot}L)/D)/V_g))(1/P_{atm})^{2.5})^{-1})^{0.5}\end{aligned} \quad (5)$$

Written in this form, the experimental model has the convenience that it can be applied to conditions of natural explosive events to check whether results are consistent with literature data.

Application of the model to natural conditions and construction of regime diagrams

To verify the applicability of our experimental model to the natural case, first some theorethical considerations are needed. The best way to understand if our experiments are in the same physical range as natural eruptions is to check, by means of some well-established non-dimensional groups from fluid dynamics, if they are in the same regime. The Reynolds number of the gas-particle mixture issuing from the conduit, $Re_{mix}=\rho_{mix}\ W_{exit}\ D\ /\mu_{mix}$, where $\mu_{mix}=\mu_g(1-C)^{-2.5}$ is the viscosity of the mixture [*Ishii and Zuber, 1979*] and μ_g is the gas viscosity, is always higher than 10^7 (see Table 3). This surely is lower than that of natural eruptions, but it is well within the range of fully turbulent flows, which are characteristic of natural events. Other than the Reynolds number, we were able to replicate by experiments other fundamental fluid-dynamic properties of the natural eruptive flows. Both pressure balanced conditions and overpressured conditions were registered at conduit exit. Also, the effect of increased buoyancy, which is characteristic of volcanic dilute columns, was observed in the hot experimental runs leading to convective plumes. Therefore, it seems that our experiments are indeed in the same regime as natural events. This finding encouraged us to apply our model to the natural conditions of explosive eruptions and check if results were consistent with literature data. For this aim we applied our experimental model to the data in *Papale,* [*2001*]. Papale's dataset includes an ample range of conditions and the conduit flow is calculated therein by means of a well-established numerical multiphase model. Comparison of data highlights (Fig.11) that our results agree on average with those of *Papale,*[*2001*] if a constant specific fragmentation energy of 2 kJ/kg is used, which is consistent with experimental values for high-silica, vesicle-rich melts [*Büttner et al., 2006*]. For some data points there is a moderate difference between the models in the value for exit velocity. We think that this difference could probably be much reduced if the fragmentation energy, which is variable over the range of natural magmas, is precisely set by data obtained with systematic experiments on fragmentation. This finding shows the importance of further research on the fragmentation mechanisms of explosive eruptions.

Finally, with the aim of checking the ability of our model to discriminate between different eruptive regimes of natural events, and to verify the significance of Ω and Γ in controlling the regime of natural explosive eruptions, we generated the diagrams of Fig.12, by applying our model to a range of natural conditions. For melt density, ρ_{melt}, we used 2500 kg/m^3, consistent with the common silica-rich compositions of explosive eruptions. Magma density is $\rho_{magma} = \rho_{melt}(1-\alpha)+\rho_{gas}\alpha$, where α is the volumetric fraction of gas bubbles in the magma and ρ_{gas} is gas density. We assumed that gas pressure inside vesicles prior to fragmentation equals magmastatic pressure at fragmentation depth. Conduit length corresponds to fragmentation depth.

Similar to what was discussed for experiments, we considered that the total mechanical energy of natural events, E_{totnat}, is the sum of two components, $E_{totnat}=E_{fragnat}+E_{exp}$, with fragmentation energy, $E_{fragnat}$, allowing acceleration of the gas particle mixture at the onset of fragmentation, and the mechanical energy derived from gas expansion after breaking of gas bubbles, E_{exp}, as contributing in sustaining the conduit flow. Mechanical energy derived from gas expansion was calculated by $E_{exp}=\rho_{magma}gLV_{Pnat}\alpha,$ where V_{Pnat} is the volume of magma (including gas bubbles) fragmented into particles. Fragmentation energy was calculated by $E_{fragnat}= SFE{*}m_{nat}$, by setting a value of 2kJ/kg for specific fragmentation energy, *SFE*, which is typical of silica-rich vesiculated magmas [*Büttner et al., 2006*]. The mass of magma fragmenting into particles is calculated by $m_{nat=} V_{pnat}\rho_{magma}$.

The regime diagrams of Fig. 12 were constructed by plotting exit velocity as a function of conduit diameter. The function was calculated by using the chosen conditions of natural events in place of the respective experimental quantities of equation (5). In particular, E_{totnat}, $E_{fragnat}$, m_{nat}, and V_{pnat}, which represent, respectively, total mechanical energy, fragmentation energy, mass of magma fragmented into particles and volume of magma fragmented into particles in natural events, were used in place of E_{tot}, E_{frag}, m and V_p, in equation (5).

With increasing particle volumetric concentration, vertically collapsing columns are favoured over convective plumes (Fig. 12A). At lower velocities, dynamic pressure decreases, and at still higher concentrations, gas overpressure increases. These are the conditions that favour radially expanding columns on the lower part of the diagram. The curves representing the eruption rate, $ER= W_{exit}(\rho_{part}C+\rho_{gas}(1-C))\pi R^2)$ of 10^7 kg/s and 10^8 kg/s, cross the limit between convective plumes and vertically collapsing columns at values of conduit diameter of about 50 m and 125 m, and exit velocities of about 230 and 255 m/s respectively, which are quite consistent with the literature [*Wilson et al., 1980*], corroborating the effectiveness of our experimental model. A decrease in conduit length and magma vesicularity, α, and an increase in particle size all favour vertically collapsing columns over convective plumes (Fig. 12A, B, C). The field of radially expanding columns is restricted to narrow conduits because, with a fixed particle volume, this is the condition leading to high particle concentration and hence high gas overpressure, at conduit exit.

Explosive eruptions are a continuum between two end members: Vulcanian and Plinian. In the first case, the eruption is short lived, the conduit flow persists for seconds up to minutes [*Wilson et* *al., 1978*] and the total volume of erupted particles rarely exceeds 10^6 m^3. In the plinian case, the conduit flow can persist for several hours or more [*Carey and Sigurdsson, 1989*] and the total volume of erupted particles can exceed 10^9 m^3. Thus if, in the Vulcanian case, the total volume of particles has already fragmented before the gas-particle flow reaches conduit exit, it is certain that in the plinian case, magma fragmentation continues long after the front of the gas-particle flow first passes the conduit exit. If the eruption rate is constant, as postulated for the sustained phase of plinian eruptions [*Carey and Sigurdsson, 1989*], particles issuing from the conduit are replaced by an equal amount of new particles generated at the fragmentation zone, and the conduit hosts a constant "control" volume of particles during the eruption. This volume, V_{pnat}, is a function of magma fragmentation speed, W_{fr}, length of fragmenting magma, L_{fr}, conduit length and conduit flow velocity, and it can be found by equating the time scale of magma fragmentation to the time scale of conduit flow, $W_{fr}/L_{fr}=W_{exit}/L$, where $L_{fr}=V_{pnat}/\pi R^2$. The few data available on fragmentation speed suggest maximum values of a few tens of m/s [*Spieler et al., 2004*]. At the intersection of the curves representing particle volume values and those representing the limits of Ω and Γ, the corresponding value of fragmentation speed is marked on figure 12E. From these values it emerges that, with a set value of particle volume, at increasing fragmentation speed vertically collapsing columns and then radially expanding columns are favoured over convective plumes. With a conduit diameter of 80 to 160 m, which is a likely range for plinian eruptions, the curve representing the limit of convective plumes (Ω= 500 s^{-1}) intersects the particle volume curves of $5x10^5$ and 10^6 m^3 respectively, which correspond to fragmentation speeds of 6.5 and 2.9 m/s, exit velocities of 255 and 245 m/s and particle discharge rates, $PDR= W_{exit}\rho_{part}C\pi R^2$, of $2x10^7$ and $3.8x10^7$kg/s. At these rates, 1 km^3 of solid material is erupted in 4.5 and 8.7 hrs respectively, which compares favourably with data from the historical plumes of Vesuvius [*Sigurdsson et al., 1985*], St. Helens [*Christiansen and Peterson, 1981*] and Pinatubo [*Paladio-Melosantos et al., 1996*]. So, even if our knowledge of fragmentation speed is "a work in progress", its influence on the eruption regime seems evident. Since fragmentation speed increases with decreasing magma vesicularity [*Koyaguchi and Mitani,* *2005; Kueppers et al., 2006*], we suggest that the tendency of poorly vesicular magmas to favour collapsing columns over convective plumes is attributable not only to a lower gas content but also to a higher fragmentation speed.

Conclusion

We conclude that our experimental model is consistent with the present knowledge of volcanology and helps interpret the regimes of explosive eruptions. It has the advantage of being very easy to use if magma properties at fragmentation (particle size, specific fragmentation energy, gas volume and pressure) and conduit geometry are known from geophysical data, or can be confidently inferred. We think that our model is a simple tool for modellers to use in setting the conditions at conduit exit of convective plumes, vertically collapsing columns and radially expanding columns, which are responsible for the main eruptive style of explosive eruptions: pyroclastic fallout, pyroclastic flows and base surges. New data, by extending the range of experimental conditions, could serve to refine model equations and regime diagrams. It is nevertheless clear from this research that magma fragmentation characteristics, i.e. speed [*Spieler et al., 2004*], energy [*Büttner et al., 2006*] and grain size [*Zimanowski et al., 2003*] are critical controls on eruption style and need further, systematic investigation.

Finally, in some of our experimental runs, overpressure was maintained up to conduit exit even if the Mach number in the mixture was much lower than 1. Based on this outcome, it seems that, especially in the case of highly concentrated mixtures, overpressured conditions can be maintained at conduit exit also in sub-sonic flows. This finding deserves further investigation in order to assess the possibility of shock-wave formation in the crater area of actual volcanoes, caused by this particular condition.

Acknowledgments. Research was partially funded by DPC-INGV agreement 07-09 and MUR PRIN 06. Michael H. Ort, James White and anonymous referee are greatly acknowledged for their thorough revision.

Reference

Büttner, R., P. Dellino, H. Raue, I. Sonder, and B. Zimanowski (2006), Stress-induced brittle fragmentation of magmatic melts: Theory and experiments, *J. Geophys. Res.*, *111*, B08204, doi:10.1029/2005JB003958.

Buresti, G., and C. Casarosa (1989), One-dimensional adiabatic flow of equilibrium gas-particle mixtures in long vertical ducts with friction, *J. Fluid Mech*., *203*, 251-272.

Burgisser, A., G. W. Bergantz, and R. E. Breidenthal (2005), Addressing complexity in laboratory experiments: the scaling of dilute multiphase flows in magmatic systems, *J. Volcanol. Geotherm. Res.*, *141*, 245-265.

Bursik, M. I., and A. W. Woods (1991), Buoyant, superbouyant and collapsing eruption columns, *J. Volcanol. Geotherm. Res.*, *45*, 347-350.

Carey, S. N., and H. Sigurdsson (1989), The intensity of plinian eruptions, *Bull. Volcanol.*, *51*, 28-40.

Christiansen, R. L., and D. W. Peterson (1981), Chronology of the 1980 eruptive activity, *U.S. Geol. Surv. Prof. Pap.*, *1250*, 17-30.

Crowe C. T. (2006), Multiphase flow handbook, Taylor & Francis Group, *LLC*.

Dellino, P., B. Zimanowski, R. Büttner, L. La Volpe, D. Mele, and R. Sulpizio (2007), Large-scale experiments on the mechanics of pyroclastic flows: Design, engineering, and first results, *J. Geophys. Res.*, *112*, B04202, doi: 10.1029/2006JB004313 (2007).

Dellino, P., D. Mele, R. Bonasia, G. Braia, L. La Volpe, and R. Sulpizio (2005), The analysis of the influence of pumice shape on its terminal velocity, *Geophys. Res. Lett.*, *32*, L21306, doi:10.1029/2005GL02395.

Dingwell, D. B. (1996), Volcanic Dilemma: Flow or Blow?, *Science*, *273*, 1054-1055.

Dobran, F., A. Neri, and G. Macedonio (1993), Numerical simulation of collapsing volcanic columns, *J. Geophys. Res. 98*(B3), 4231-4259.

Garic, R. V., Z. B. Grbavcic, and S. Dj. Jovanovic (1995), Hydrodynamic modeling of vertical non-accelerating gas-solids flow, *Powder Technol.*, *84*, 65-74.

Ishii, M., and N. Zuber (1979), Drag coefficient and relative velocity in bubbly, droplet or particulate flows, *AIChE J.*, *25*, 843-855.

Koyaguchi, T., and N. K. Mitani (2005), A theoretical model for fragmentation of viscous bubbly magmas in shock tubes, *J. Geophys. Res. 110*(B10202), doi:10.1029/2004JB003513.

Kueppers, U., B. Scheu, O. Spieler, and D. B. Dingwell (2006), Fragmentation efficiency of explosive volcanic eruptions: A study of experimentally generated pyroclasts, *J. Volcanol. Geotherm. Res.*, *153*, 125-135.

Kulick, J.D., J.R. Fessler, and J.K. Eaton, (1994), Particle response and turbulence modification in fully developed channel flow, *J. Fluid Mech.*, *277*, 285–309.

Mader, H. M., E. E. Brodski, D. Howard, and B. Sturtevant (1996), Laboratory simulations of sustained volcanic eruptions, *Nature*, *388*, 462-464.

Ogden, D. E., G. A. Glatzmaier, and K. H. Wohletz (2008), Effects of vent overpressure on buoyant eruption columns: Implications for plume stability, *Earth Plan. Sci. Lett.*, *268*, 283-292, doi:10.1016/j.epsl.2008.01.014.

Ogden, D. E., K. H. Wohletz, G. A. Glatzmaier, and E. E. Brodsky (2008), Numerical simulations of volcanic jets: Importance of vent overpressure, *J. Geophys. Res.*, *113*, B02204, doi:10.1029/2007JB005133.

Paladio-Melosantos, M. L. O., R. U. Solidum, W. E. Scott, R. B. Quiambao, J. V. Umbal, K. S. Rodolfo, B. S. Tubianosa, P. J. Delos Reyes, R. A. Alonso, and H. B. Ruelo (1996), Tephra falls of the 1991 eruptions of Mount Pinatubo, *in* Newhall, C. G., and R. S. Punongbayan, Eds., Fire and Mud: Eruptions and Lahars of Mount Pinatubo, Philippines, (Philippine Institute of Volcanology And Seismology, Quezon City, Univ. of Washington Press, Seattle,1996), pp. 687-731.

Papale P. (1999), Strain-induced magma fragmentation in explosive eruptions, *Nature*, *397*, 425-428.

Papale P. (2001), Dynamics of magma flow in volcanic conduits with variable fragmentation efficiency and nonequilibrium pumice degassing, *J. Geophys. Res*., *106*(B6), 11043-11065.

Sigurdsson, H., S. Carey, W. Cornell, and T. Pescatore (1985), The eruption of Vesuvius in AD 79, *Nat. Geogr. Res.*, *1*, 332-387.

Spieler, O., D. B. Dingwell, and M. Alidibirov (2004), Magma fragmentation speed: an experimental determination, *J. Volcanol. Geotherm. Res.*, *129*, 109-123.

Valentine, G. A., and K. H. Wohletz (1989), Numerical models of plinian eruption columns and pyroclastic flows, *J. Geophys Res. 94*(B2), 1867-1887.

Wilson, L., R. S. J. Sparks, and G. P. L. Walker (1980), Explosive volcanic eruption – IV. The control of magma properties and conduit geometry on eruption column behaviour, *Geophys. J. R. Astr. Soc.*, *63*, 117-148.

Wilson, L., R. S. J. Sparks, T. C. Huang, and N. D. Watkins (1978), The control of volcanic column heights by eruption energetics and dynamics, *J. Geophys. Res. 83*, 1829-1836.

Wohletz, K.H. (1998), Pyroclastic surges and compressible two-phase flows, *in* Freundt A, and M. Rosi , Eds., From magma to tephra, Elsevier, Amsterdam.

Woods, A. W. (1988), The fluid dynamics and thermodynamics of eruption columns, *Bull. Volcanol.*, *50*, 169-193.

Woods, A. W. (1995a), The dynamics of explosive volcanic eruptions, *Rev. Of Geophys.*, *33*, 495-530.

Zimanowski, B., K. Wohletz, P. Dellino, and R. Büttner (2003), The volcanic ash problem, *J. Volcanol. Geotherm. Res.*, *122*, 1-5.

Figure captions

Figure 1. Experiment design and parts. **A**, sketch (modified after *Dellino et al.,* [*2007*]) of the experimental apparatus. **B**, mounting operation inside the pit where the base-plate of the conduit is located. The solenoid valves that initiate gas transfer from the gas reservoirs (30 m long tubes of fig 1A), the location of the sensors for measuring the driving pressure and the base plate of the conduit are shown. **C**, conduit mounted in a configuration allowing a dense network of sensors for measuring pressure during the conduit flow. Sensor locations are shown. The first sensor is placed at a level that is always completely filled by particles. With this sensor the amount of energy transferred to the particles prior to system expansion can be calculated (see Fig. 2). Other sensors allow measuring the speed of the gas particle flow when particle concentration is very high (see Fig. 2), or the speed of sound of the gas-particle system when particle concentration is lower (Fig. 4).

Fig. 2. Diagram showing normalized pressure signals measured at a high sampling rate during an experiment with a high particle load, performed with multiple pressure sensors. The solid black line is the signal of the driving pressure recorded from the sensor placed between the gas reservoir and the nozzles. The area under this curve allows measurement of the mechanical energy transferred to particles over time. The time-lag between onset of driving pressure and system expansion, as registered by the peak of the first sensor in the conduit, allows measurement of the mechanical energy transferred to the particles and impulsively released at initiation of particle motion, which is analogous to fragmentation energy. Dashed lines represent the pressure signal recorded by sensors placed at various heights along the conduit. Pressure peaks register the arrival of the gas-particle flow. The time-lag between peaks indicates the velocity of the gas-particle flow inside the conduit. Videocameras pointing directly at the conduit exit reveal the velocity of the gas-particle flow at conduit exit, and matching of this data with internal velocity.

Fig. 3. Cartoons showing the evolution of the gas-particle flow inside the conduit for dilute and concentrated runs. **A,** the particle load is low and the flow reach dilute condition in the conduit,

which allow effective percolation of gas through the mixture and upward the conduit. **B,** the particle load is high and the flow is highly concentrated. Perculation of gas through the mixture up in the conduit is in part inhibited. This condition allows to maintain overpressure at conduit exit.

Fig. 4. Diagrams showing normalized pressure signals recorded by two sensors during two experiments with a lower particle load compared with the experiment of fig. 2. **A**, Particle volumetric concentration, *C*, is about 0.12. The distance between sensors is 0.8 m, while the time difference between pressure peaks is about 0.03 s. The speed of sound of the mixture is about 27 m/s, which is much higher than the exit velocity of the gas-particle mixture (9.9 m/s) as recorded by the videocamera. **B,** Particle volumetric concentration, *C*, is about 0.04. The distance between sensors is 1.65 m, while the time difference between pressure peaks is about 0.015 s. The speed of sound of the mixture is about 110 m/s.

Fig. 5. A sequence of images taken from an experiment producing a convective plume. **A**, initiation of the plume at conduit exit. **B**, ascent and expansion of the plume. **C**, further expansion of the plume and initiation of coarse-particle decoupling from the margin. **D**, final vertical ascent and expansion of the plume with fallout of coarse particles from the diluted plume margin.

Fig. 6. A sequence of images taken from an experiment producing a vertically collapsing column. **A**, initiation of the vertical column at conduit exit. **B**, initiation of column collapse. **C**, impact of the dense collapsing column on the ground and initiation of a density current. **D**, propagation of the density current, which resembles a natural pyroclastic flow.

Fig. 7. A, sequence of images taken from an experiment producing a radially expanding column. **A**, formation of a radially expanding column at conduit exit. **B**, further radial expansion of the

column. **C**, diluted collapse of the expanded column. **D**, density current, resembling a natural base surge, forming after the dilute collapse.

Fig. 8. A sequence of images comparing a hot and a cold experiment producing convective plumes. **A** and **B**, initial plume formation of a hot experiment. **C**, initial plume formation of a cold experiment. **D** and **E**, further plume ascent and expansion of a hot experiment. **F**, further plume ascent and expansion of a cold experiment. The difference between **E** and **F** is height and final expansion of the plume, which is aided by higher temperature in **E**. On the right side of **A** and **D** (taken from thermal videocamera recordings), the temperature scale in °C is shown.

Fig. 9. Ω (vorticity factor) – Γ (overpressure factor) regime diagram. Data points represent all the experiments of the research and allowed us to define the limit of stability fields of convective plumes, vertically collapsing columns and radially expanding columns. Convective plumes form when $\Omega > 500\ s^{-1}$. Vertically collapsing columns occur with $\Omega < 500\ s^{-1}$. Radially expanding columns form when $\Gamma > 0.3$.

Fig. 10. Diagrams showing data correlations used for development of the experimental model. The linear functional relations and the correlation coefficients, *r*, are inset. **A**, functional relation of exit velocity, W_{exit}. **B**, functional relation of exit energy, E_{exit} (energy transferred before conduit exit). **C**, functional relation of exit pressure, P_{exit}.

Fig. 11. Diagram comparing conduit exit velocity, W_{exit} as calculated by *Papale* ,[*2001*] and by applying our model to the *Papale* [*2001*] dataset.

Fig. 12. Regime diagrams obtained by applying our experimental model equation (5) to a range of natural conditions. Diagrams show how conduit exit velocity, W_{exit} varies as a function of conduit

diameter, *D* and other eruption parameters. As melt density, ρ_{melt}, a value of 2500 kg/m^3 is always used. In the insets other parameters are defined. The dashed lines separate the stability fields of convective plumes, vertically collapsing columns and radially expanding columns and are calculated by considering the limit of the vorticity factor (Ω=500 s^{-1}) and of the overpressure factor (Γ=0.3) as obtained by the experimental regime diagram of Fig. 9. **A**, the solid black curves represent W_{exit} as a function of *D* for various values of particle volumetric concentration, *C*. The bold dashed lines curves represent eruption rates, *ER*, of 10^7 kg/s and 10^8 kg/s respectively. **B**, the solid black curves represent W_{exit} as a function of *D* for various values of conduit length, *L*. **C**, the solid black curves represent W_{exit} as a function of *D* for various values of particle median size normalized to 1 mm, d_p. **D**, the solid black curves represent W_{exit} as a function of *D* for various values of magma vesicularity, α. **E**, the solid black curves represent W_{exit} as a function of *D* for various values of volume of magma fragmented into particles, V_{pnat}. Fragmentation speed values, W_{fr}, are reported at the intersection of the V_{pnat} curves with both the boundary between the convective plumes and vertically collapsing columns, and the boundary between the vertically collapsing columns and the radially expanding columns. Particle discharge rates corresponding to the limit between collapsing columns and convective plumes are marked (inclined segments) for conduit diameters of 80 and 160 m respectively.

Table 1. Range of experimental conditions

Conduit diameter (D) m	Conduit length (L) m	Pressurized gas volume litres	Gas overpressure bar	Particle load (m) kg	Particle median size normalized to one mm (d_p) -	Temperature °C
0.3 - 0.6	0.55 - 3.2	1.5 - 14	90 - 180	13 - 220	0.5 - 1.5	20 -300

Table 2. List of symbols and description.

Symbol	description	dimension
α	Vesicularity (volumetric fraction of gas bubbles in the magma)	-
Γ	Overpressure factor (Γ=P_{over}/P_{dyn})	-
C	Particle volumetric concentration ($C= V_p /V$)	-
D	Conduit diameter	m
ΔP_{init}	Initial gas ovepressure of experiments	Pa
d_p	Particle median diameter normalized to 1 mm	-
d	Particle diameter	m
E_{exit}	Energy transferred before conduit exit of experiments	J
E_{exp}	Mechanical energy derived from expanding gas from broken gas bubbles of natural events ($E_{exp}=\rho_{magma}gLV_P\alpha$)	J
$E_{fragexp}$	Fragmentation energy of experiments	J
$E_{fragnat}$	Fragmentation energy of natural events ($E_{fragnat}=SFE*m$)	J
E_{totexp}	Total mechanical energy of experiments ($E_{totexp}=\Delta P_{init}\ V_{ginit}$)	J
E_{totnat}	Total mechanical energy of natural events ($E_{totnat}=E_{fragnat}+E_{exp}$)	J
ER	Eruption rate of natural events ($ER= W_{exit}(\rho_{part}C+\rho_{gas}(1-C))\pi R^2$)	kg/s
g	Gravity acceleration	9.81 m/s^2
L	Conduit length	m
L_{fr}	Length of fragmenting magma of natural events ($L_{fr} = V_{pnat}/\pi R^2$)	m
m	Particle load of experiment	kg
m_{nat}	Mass of magma fragmented into particles of natural events ($m_{nat=}\ V_{pnat}\rho_{magma}$)	kg
μ_{mix}	Viscosity of the gas-particle mixture	Pa s
μ_g	Gas viscosity	Pa s
P_{atm}	Atmospheric pressure	10^5Pa
P_{dyn}	Dynamic pressure of experiments along vertical axis ($P_{dyn}=0.5\rho_{mix}\ W_{exit}^2$)	Pa
P_{exit}	Pressure at conduit exit of experiments	Pa
P_{over}	Exit ovepressure ($P_{over}= P_{exit}- P_{atm}$)	Pa
PDR	Particle discharge rate of natural events ($PDR= W_{exit}\rho_{part}C\pi R^2$)	kg s^{-1}
R	Conduit radius	m
Re_{mix}	Reynolds number of the gas particle mixture ($Re_{mix}=\rho_{mix}\ W_{exit}\ D\ /\mu_{mix}$)	-
ρ_{gas}	Gas density	kg/m^3
ρ_{magma}	Magma density ($\rho_{magma} = \rho_{melt}(1- \alpha)+ \rho_{gas}\alpha$)	kg/m^3
ρ_{melt}	Melt density (density of vesicle free magma)	kg/m^3
ρ_{mix}	Gas-particle mixture density ($\rho_{mix}= \rho_{part}C+\rho_{gas}(1-C)$)	kg/m^3
ρ_{part}	Particle density	kg/m^3
SFE	Specific Fragmentation Energy	J/kg
SME	Specific mechanical energy of experiments ($SME=E_{totexp}/m$)	J/kg
V	Conduit volume (V_p+V_g)	m^3
V_g	Conduit gas volume	m^3
V_{ginit}	Reservoir gas volume of experiments	m^3
V_p	Volume of particles in experiments	m^3
V_{pnat}	Volume of magma fragmented into particles of natural events	m^3
w	Particle terminal velocity	m/s
W_{exit}	Velocity at conduit exit	m/s
W_{fr}	Magma fragmentation speed	m/s
W_{int}	Internal velocity (Velocity of the gas particle mixture inside the conduit)	m/s
Ω	Vorticity factor ($\Omega=2W_{exit}/CR$)	s^{-1}

Table 3. Experiment data used for the calculation of the Reynolds number. VCC = vertically collapsing columns; TRANS = transitional columns; CP = convective plumes; REC= radially expanding columns.

Regime	Mixture density ρ_{mix} kg m^{-3}	exit velocity W_{exit} m s^{-1}	Cond. Diam. D m	Particle Volum. conc. C -	mixture viscosity μ_{mix} Pa s	Reynolds number mixture Re_{mix} -
VCC	266.52	9.45	0.6	0.171	2.88E-05	5.25E+07
TRANS	291.36	11.00	0.6	0.187	3.02E-05	6.37E+07
VCC	378.97	11.45	0.6	0.243	3.62E-05	7.20E+07
CP	108.23	14.46	0.6	0.069	2.15E-05	4.36E+07
VCC	430.16	12.56	0.6	0.276	4.04E-05	8.02E+07
VCC	434.66	12.03	0.6	0.279	4.08E-05	7.68E+07
VCC	314.07	10.23	0.6	0.202	3.16E-05	6.10E+07
VCC	484.03	11.26	0.6	0.311	4.57E-05	7.16E+07
REC	585.88	10.23	0.6	0.377	5.87E-05	6.12E+07
CP	102.44	16.95	0.6	0.065	2.13E-05	4.89E+07
REC	526.44	9.23	0.6	0.338	5.06E-05	5.76E+07
REC	470.47	7.01	0.3	0.302	4.43E-05	2.23E+07
REC	454.92	8.78	0.3	0.292	4.27E-05	2.81E+07
REC	457.75	6.32	0.3	0.294	4.30E-05	2.02E+07
REC	452.10	8.67	0.3	0.291	4.25E-05	2.77E+07
CP	170.77	12.54	0.3	0.109	2.40E-05	2.67E+07
CP	204.70	13.23	0.3	0.131	2.56E-05	3.18E+07
CP	184.91	10.56	0.3	0.118	2.47E-05	2.38E+07
REC	450.68	8.07	0.3	0.290	4.23E-05	2.58E+07
VCC	453.51	6.67	0.3	0.291	4.26E-05	2.13E+07
CP	199.05	15.46	0.3	0.127	2.53E-05	3.65E+07
REC	453.51	7.339	0.3	0.291	4.26E-05	2.34E+07
VCC	322.42	12.10	0.6	0.207	3.21E-05	7.28E+07
CP	184.91	11.67	0.3	0.118	2.47E-05	2.62E+07
VCC	222.02	10.95	0.6	0.142	2.64E-05	5.52E+07
CP	93.02	9.90	0.3	0.059	2.10E-05	1.32E+07
VCC	429.52	11.12	0.6	0.276	4.04E-05	7.10E+07
REC	467.64	6.95	0.3	0.301	4.40E-05	2.22E+07
REC	643.71	10.33	0.6	0.414	6.85E-05	5.82E+07
REC	467.64	5.10	0.3	0.301	4.40E-05	1.62E+07
REC	1177.10	7.73	0.6	0.758	6.24E-04	8.75E+06
CP	184.84	8.72	0.3	0.176	2.92E-05	1.66E+07
CP	45.31	18.33	0.6	0.028	1.93E-05	2.57E+07
REC	1112.80	8.34	0.6	0.716	4.20E-04	1.33E+07

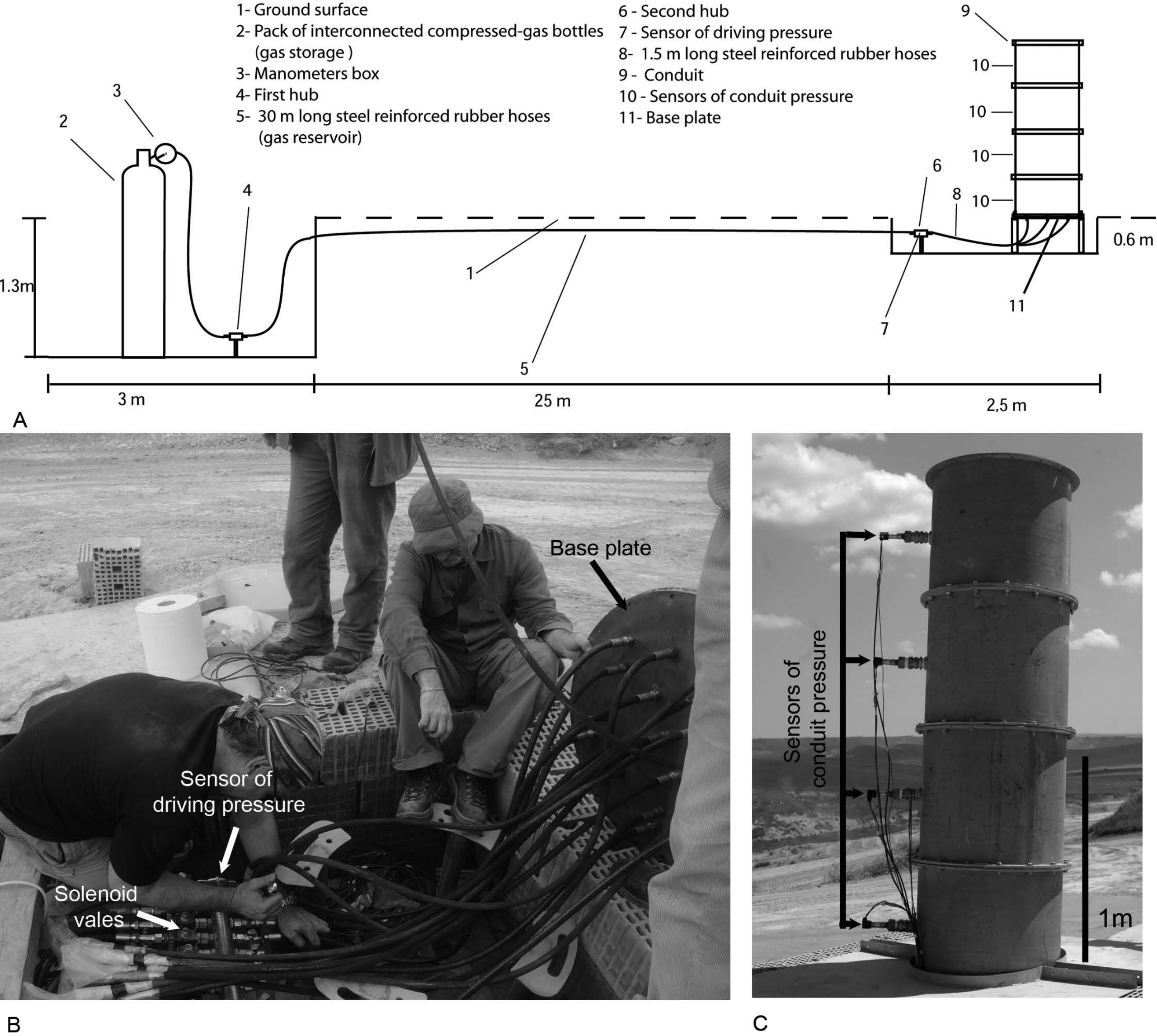
1- Ground surface
2- Pack of interconnected compressed-gas bottles (gas storage)
3- Manometers box
4- First hub
5- 30 m long steel reinforced rubber hoses (gas reservoir)
6 - Second hub
7 - Sensor of driving pressure
8- 1.5 m long steel reinforced rubber hoses
9 - Conduit
10 - Sensors of conduit pressure
11- Base plate
1.3m
0.6 m
3 m
25 m
2,5 m
A
Base plate
Sensor of driving pressure
Solenoid vales
B
Sensors of conduit pressure
1m
C

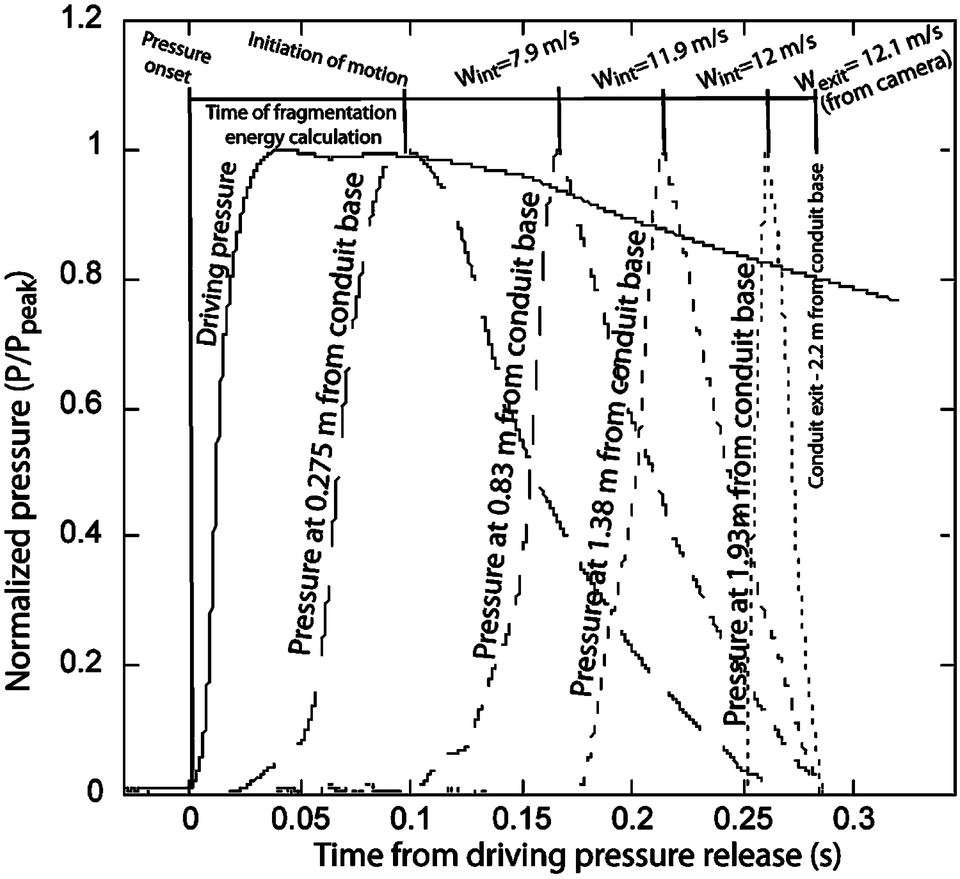
Pressure onset
Initiation of motion
Wint=7.9 m/s
Wint=11.9 m/s
Wint=12 m/s
Wexit= 12.1 m/s (from camera)
Time of fragmentation energy calculation
Driving pressure
Pressure at 0.275 m from conduit base
Pressure at 0.83 m from conduit base
Pressure at 1.38 m from conduit base
Pressure at 1.93 m from conduit base
Conduit exit - 2.2 m from conduit base
Normalized pressure (P/Ppeak)
Time from driving pressure release (s)
1.2
1
0.8
0.6
0.4
0.2
0
0.05
0.1
0.15
0.2
0.25
0.3

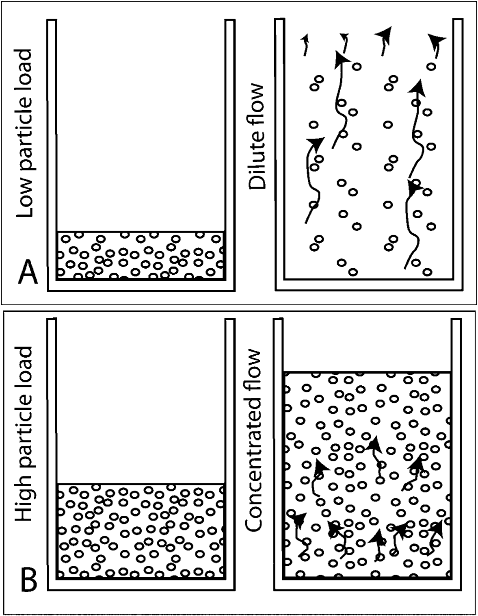
A
Low particle load
Dilute flow
B
High particle load
Concentrated flow

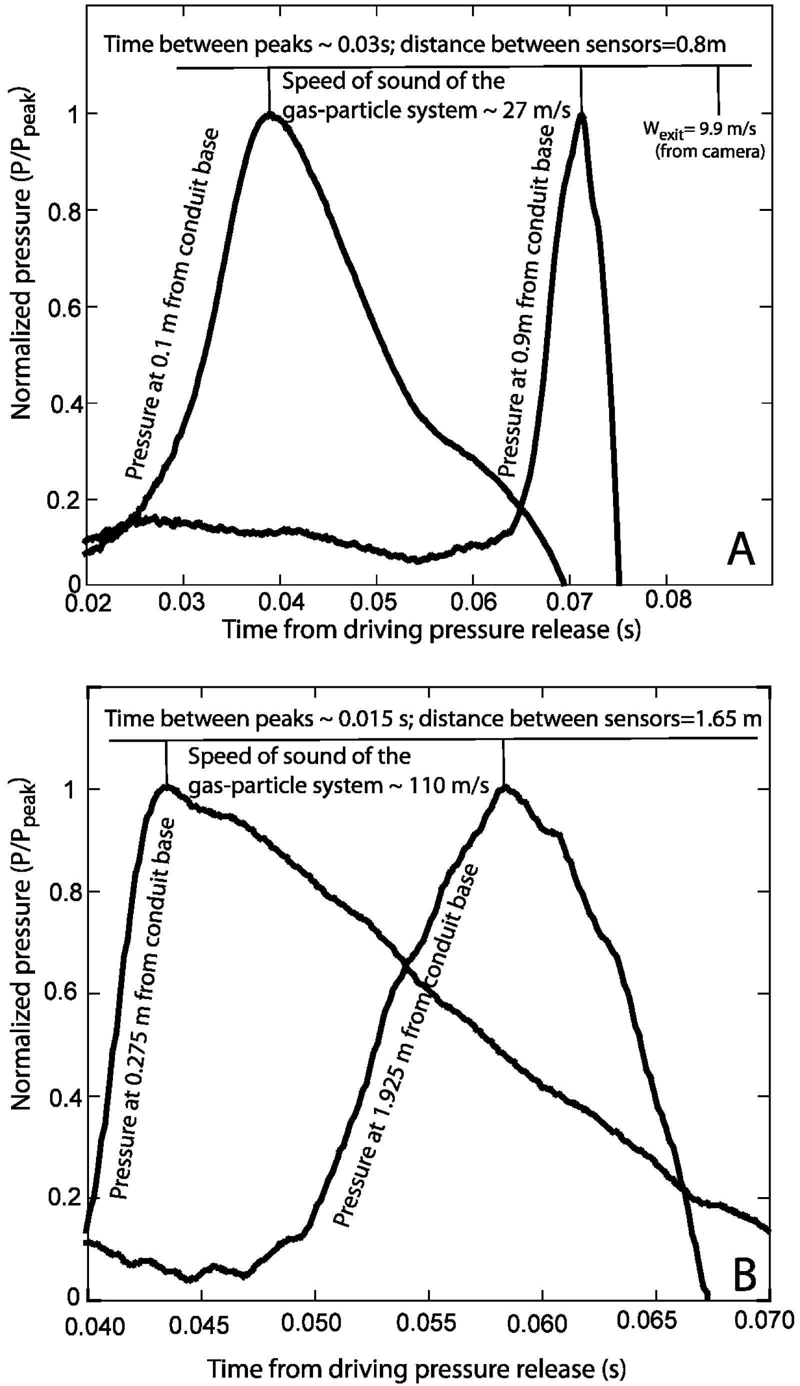
Time between peaks ~ 0.03s; distance between sensors=0.8m
Speed of sound of the gas-particle system ~ 27 m/s
W_exit= 9.9 m/s (from camera)
Pressure at 0.1 m from conduit base
Pressure at 0.9m from conduit base
Normalized pressure (P/P_peak)
Time from driving pressure release (s)
A
Time between peaks ~ 0.015 s; distance between sensors=1.65 m
Speed of sound of the gas-particle system ~ 110 m/s
Pressure at 0.275 m from conduit base
Pressure at 1.925 m from conduit base
Normalized pressure (P/P_peak)
Time from driving pressure release (s)
B

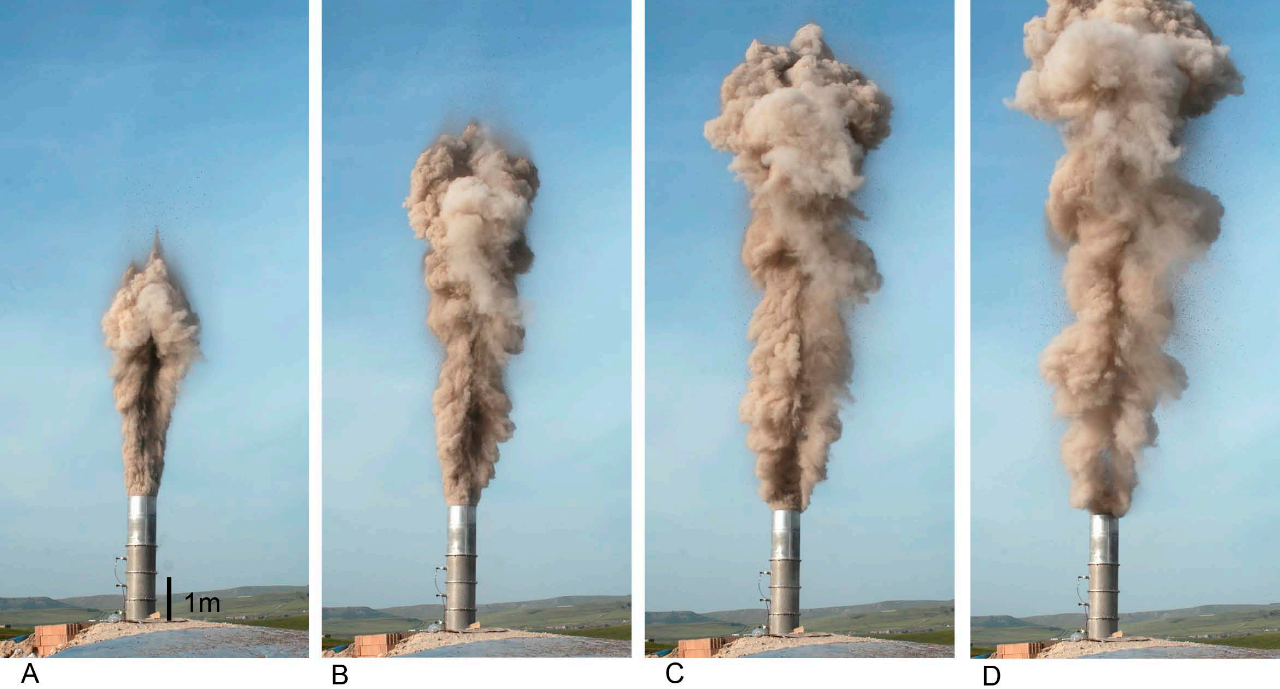
1m
A
B
C
D

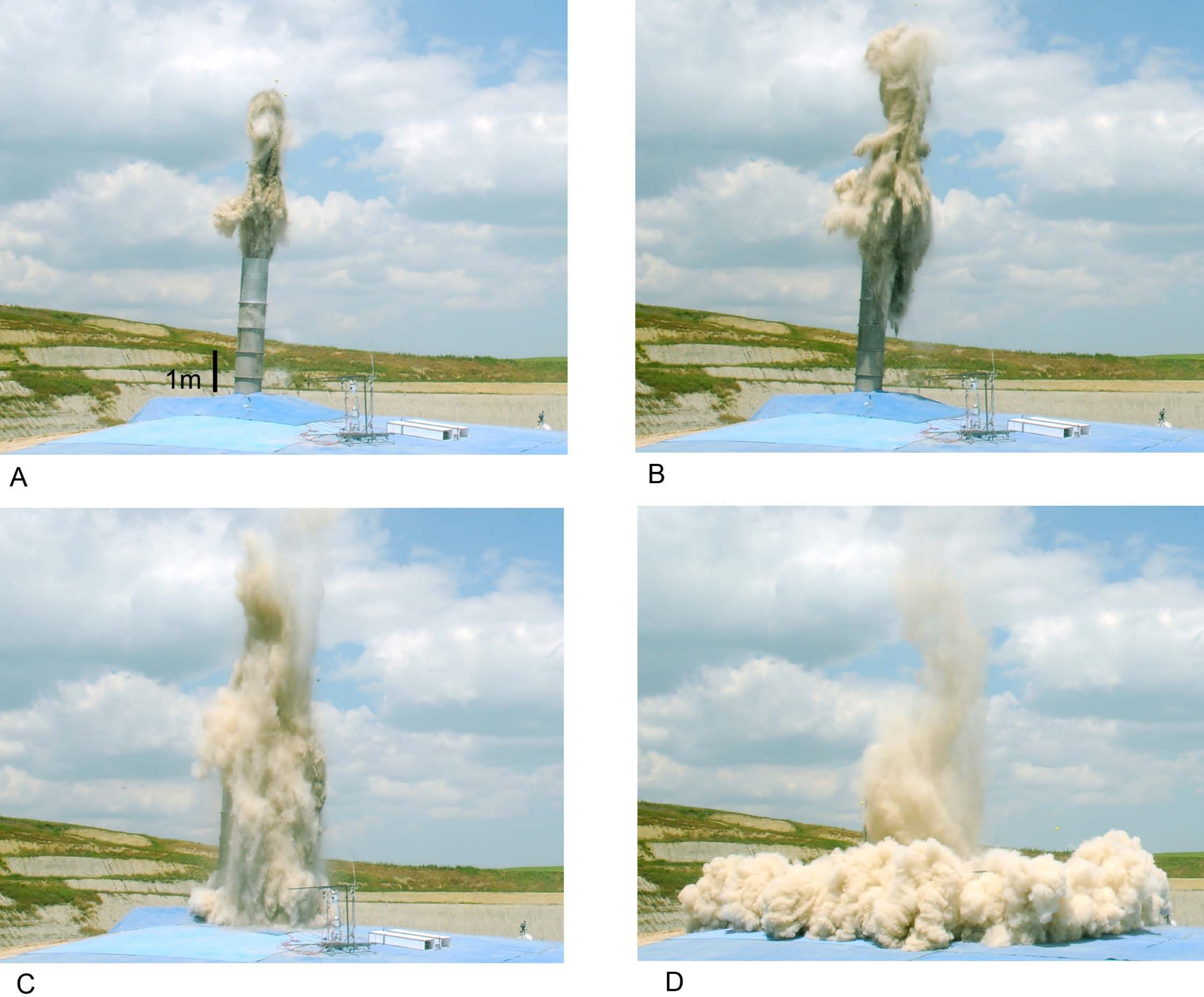
1m
A
B
C
D

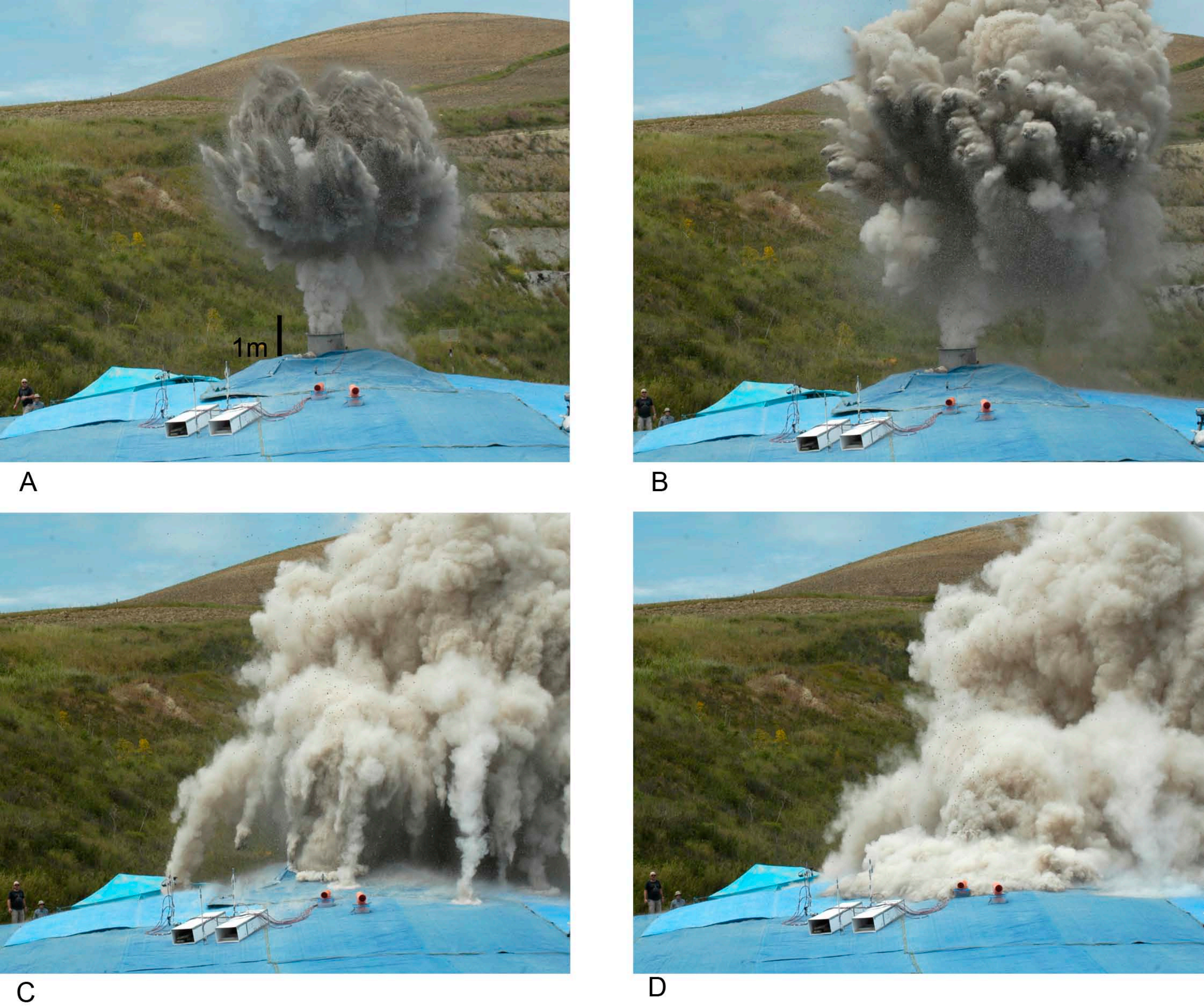
1m
A
B
C
D

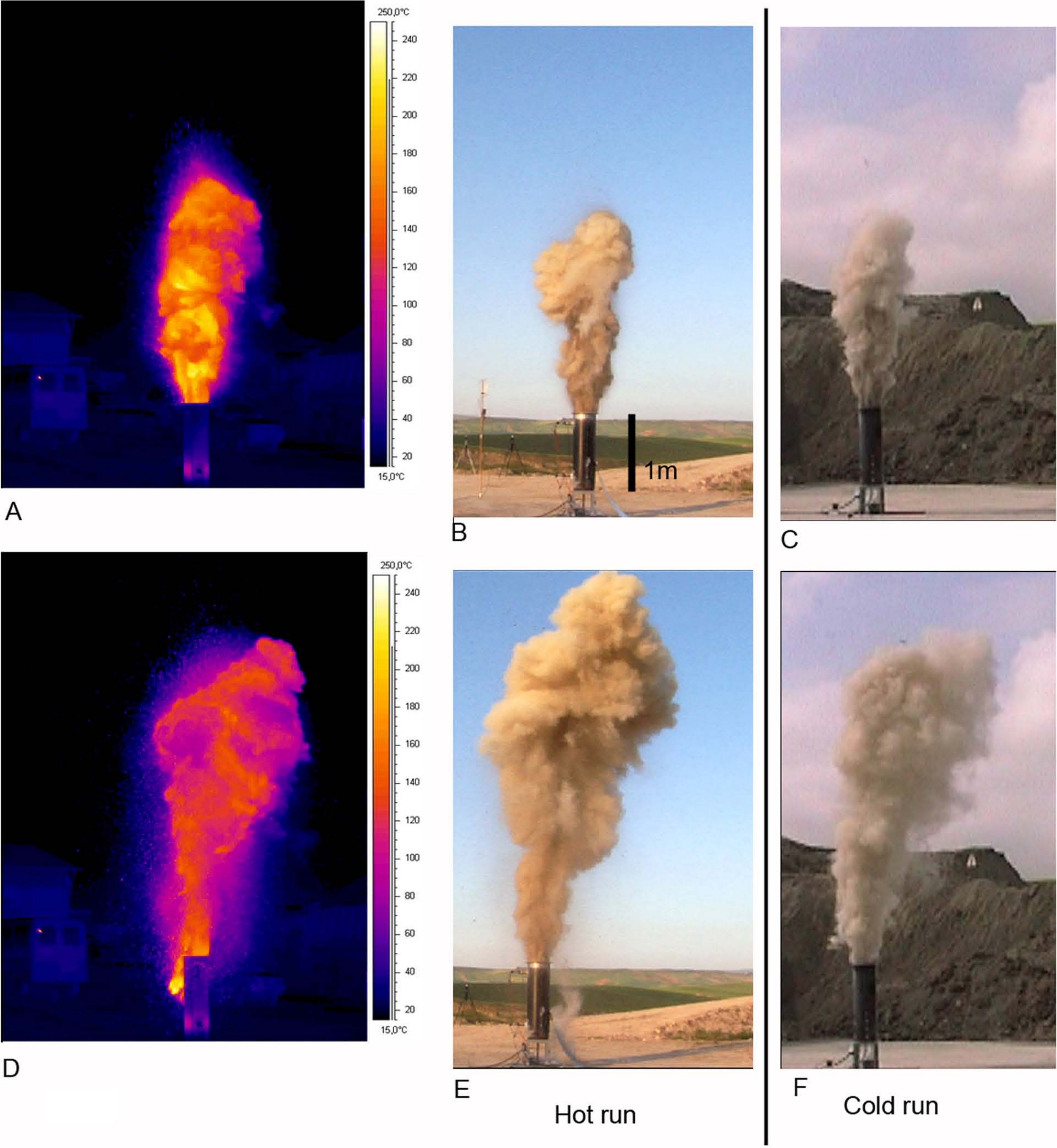
250,0°C
240
220
200
180
160
140
120
100
80
60
40
20
15,0°C
1m
A
B
C
D
E
F
Hot run
Cold run

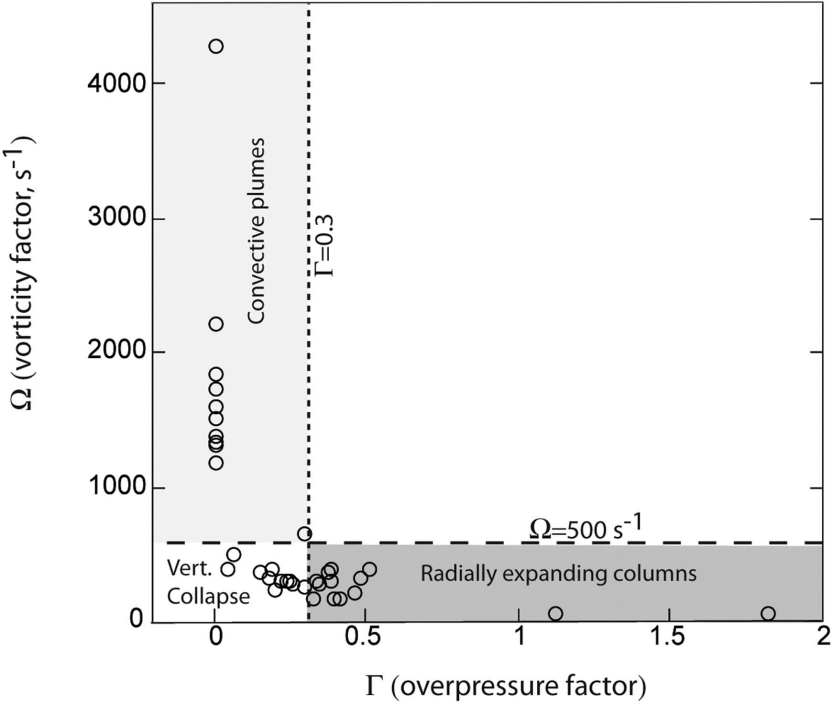

Convective plumes
Γ=0.3
Ω=500 s^-1
Vert. Collapse
Radially expanding columns
Ω (vorticity factor, s^-1)
Γ (overpressure factor)
0
1000
2000
3000
4000
0
0.5
1
1.5
2

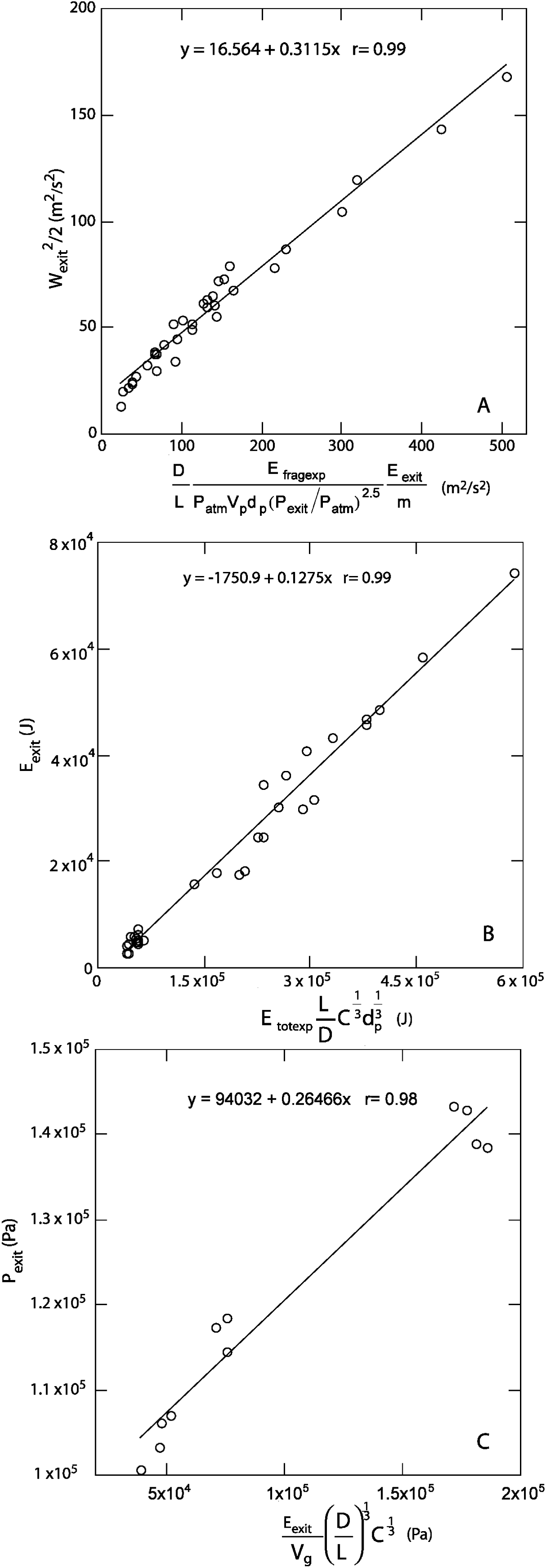

y = 16.564 + 0.3115x r= 0.99
W_exit^2/2 (m^2/s^2)
D/L · E_fragexp / (P_atm V_p d_p (P_exit/P_atm)^2.5) · E_exit/m (m^2/s^2)
A
y = -1750.9 + 0.1275x r= 0.99
E_exit (J)
E_totexp (L/D) C^(1/3) d_p^(1/3) (J)
B
y = 94032 + 0.26466x r= 0.98
P_exit (Pa)
E_exit/V_g (D/L)^(1/3) C^(1/3) (Pa)
C

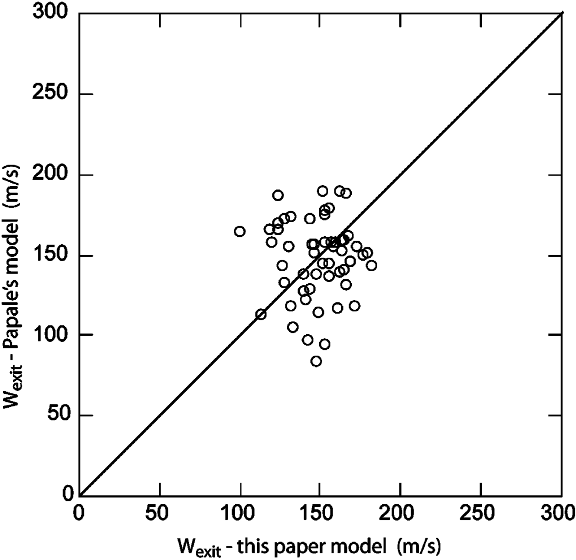

300
250
200
150
100
50
0
0
50
100
150
200
250
300
W_exit - Papale's model (m/s)
W_exit - this paper model (m/s)

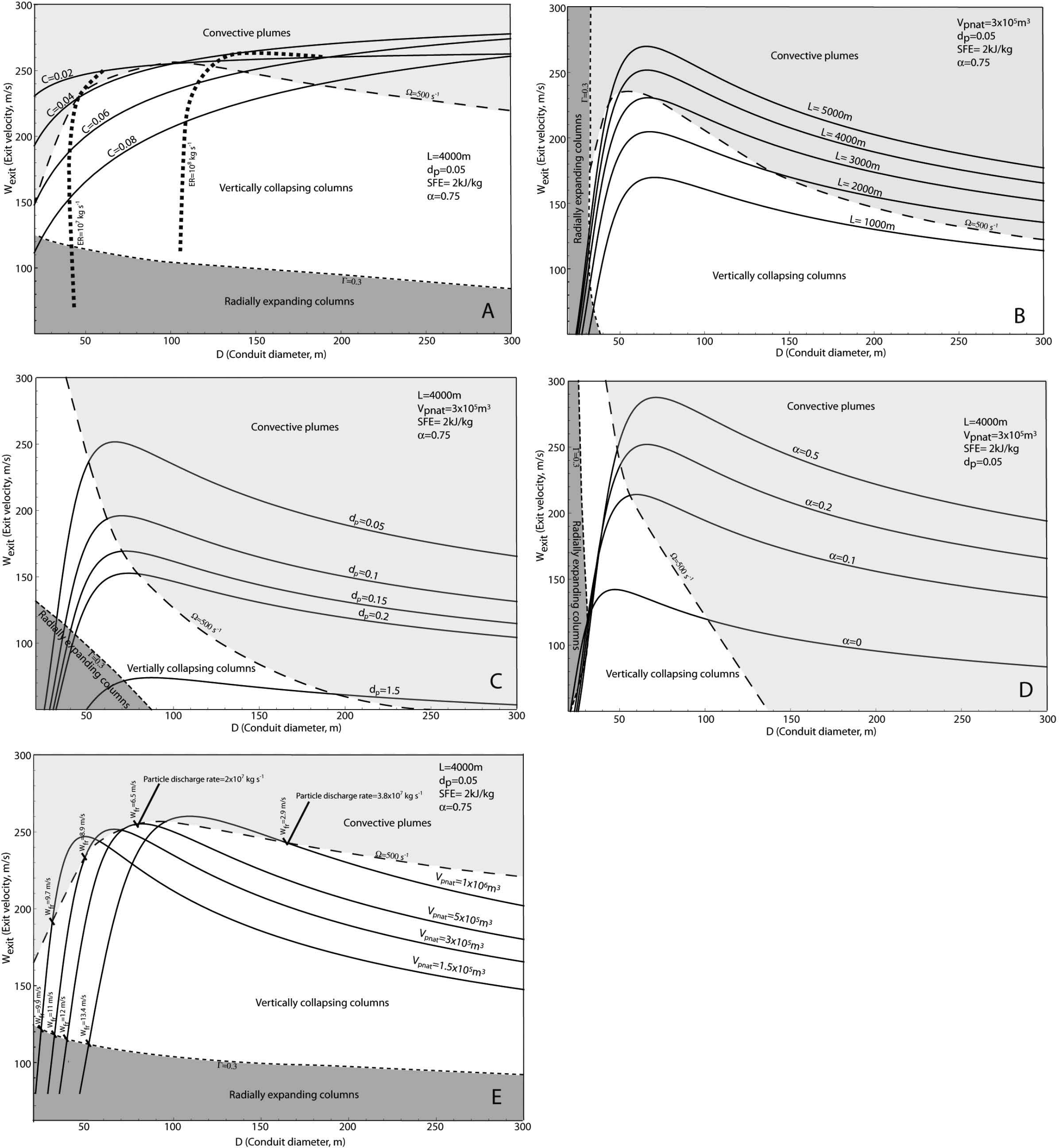
Convective plumes
C=0.02
C=0.04
C=0.06
C=0.08
Ω=500 s⁻¹
ER=10⁷ kg s⁻¹
ER=10⁸ kg s⁻¹
L=4000m
dp=0.05
SFE= 2kJ/kg
α=0.75
Vertically collapsing columns
Γ=0.3
Radially expanding columns
A
Wexit (Exit velocity, m/s)
D (Conduit diameter, m)
Vpnat=3x10⁵m³
dp=0.05
SFE= 2kJ/kg
α=0.75
L= 5000m
L= 4000m
L= 3000m
L= 2000m
L= 1000m
Radially expanding columns
B
L=4000m
Vpnat=3x10⁵m³
SFE= 2kJ/kg
α=0.75
dp=0.05
dp=0.1
dp=0.15
dp=0.2
dp=1.5
Vertially collapsing columns
C
L=4000m
Vpnat=3x10⁵m³
SFE= 2kJ/kg
dp=0.05
α=0.5
α=0.2
α=0.1
α=0
D
L=4000m
dp=0.05
SFE= 2kJ/kg
α=0.75
Particle discharge rate=2x10⁷ kg s⁻¹
Particle discharge rate=3.8x10⁷ kg s⁻¹
Wfr=6.5 m/s
Wfr=8.9 m/s
Wfr=9.7 m/s
Wfr=2.9 m/s
Wfr=9.9 m/s
Wfr=11 m/s
Wfr=12 m/s
Wfr=13.4 m/s
Vpnat=1x10⁶m³
Vpnat=5x10⁵m³
Vpnat=3x10⁵m³
Vpnat=1.5x10⁵m³
E